Lithos 320–321 (2018) 49–61

Contents lists available at ScienceDirect

Lithos

journal homepage: www.elsevier.com/locate/lithos

Mechanical and structural consequences of magma differentiation at ascent conduits: A possible origin for some mafic microgranular enclaves in granites

Carlos Fernández *, Antonio Castro

Departamento de Ciencias de la Tierra, Universidad de Huelva, 21071 Huelva, Spain

ARTICLE INFO

Article history:
Received 26 January 2018
Accepted 5 September 2018
Available online 10 September 2018

Keywords:
Mafic enclaves
Granite
Ascent conduits
Viscosity profile
Flow structures

ABSTRACT

This work evaluates the origin of mafic microgranular enclaves in granites through a process of magma splitting at the boundaries of ascent conduits, where an intermediate, high-silica andesite magma separates into two magma systems without a continuous change, one of Qz-dioritic composition and high-crystal content and another one of granite (sensu *lato*) composition and mostly liquid. Asemi-quantitative approximation considering the balance between advective and diffusive heat transfer has been followed, considering an order of magnitude procedure to estimate the thickness of the thermal boundary layer within an instantaneously emplaced dike. The resulting temperature gradient across the dike, and the expected geochemical variation evidenced by previous experimental results, have been used to determine crystallinity, viscosity, flow velocity, and shear stress profiles at a single transverse section, at 500 MPa of lithostatic pressure. The Qz-dioritic magma generated at the borders of the dike develops a strong crystallinity gradient, with a mafic chilled margin near the external contact of the dike, while crystal fraction remains very low (<10 vol%) in the differentiated granitic melt in the dike interior. The mafic chilled margin has a predominantly brittle behavior and can be broken by movement of the dike and host rock into fragments of sizes comparable to those observed in nature. Reheating and remelting of dike walls generates a strong decrease in the viscosity of the mush close to the internal geochemical contact with the granitic melt. This process leads to the formation of highly deformable channels that can entrain fragments of the previous chilled margin giving place to schlieren and enclave swarms, among many other structures. The process can be repeated through the sequential ascent of distinct magma batches transporting the mafic enclaves up to their final level of emplacement in granitic plutons and batholiths.

1. Introduction

Mafic microgranular enclaves and monogenic swarms are characteristic features of I-type granites, whose origin has been widely debated. They have been considered as either external o cogenetic to its host granite (see, e.g.,Castro etal., 2008 and references therein). In turn, cogenetic enclaves can have a restitic (e.g.,White etal., 1999) or an igneous origin (like the autoliths of e.g. Fershtater and Borodina, 1977). The processes leading to the interaction between enclaves and host can occur at any depth from the source region, through the ascent conduit, to the emplacement level (Barbarin, 2005; Barbarin and Didier, 1992). Mixing and mingling of distinct coeval magmas have been commonly cited as relevant processes to understand the geometrical and geochemical relations of mafic microgranular enclaves and host granites (Barbarin and Didier, 1991; Frost and Mahood, 1987; Vernon, 1983). The physical mechanisms proposed for the formation of mafic enclaves and swarms are very varied, including the disruption of synplutonic dikes (e.g.,Fernandez and Barbarin, 1991; Pitcher, 1991), forcible injection of mafic magma (e.g.,Sparks etal., 1977), large-scale convective instabilities (e.g.,Huppert etal., 1984; Paterson, 2009), top-to-down intrusions related to gravity instabilities and sinking enclaves (Castro etal., 2008; Wiebe etal., 2006), and processes related to crystallization at the walls of ascent conduits (Donaire etal., 2005). In the sense of the last mentioned mechanism, some enclaves have been recently interpreted by Rodríguez and Castro (2017, 2018) as magmatic to nearly solid fragments dragged from the chilled margins that form at the sidewall of magma ascent conduits. Although that genetic mechanism is supported by geochemical and experimental data (Rodríguez and Castro, 2107 and references herein), a mechanical analysis is pending. This work attempts to gain some insight into the physical feasibility and constraints on the generation of enclaves and enclave swarms at the sidewalls of magma conduits. Here, the ascent conduits are treated as feeder dikes for simplicity reasons. The analysis of the coupled mechanical and thermal evolution of dikes is in its infancy. No analytical solution is available that simultaneously accounts for

* Corresponding author.
E-mail address: fcarlos@uhu.es (C. Fernández).

https://doi.org/10.1016/j.lithos.2018.09.004
0024-4937/

equations of elasticity, fluid mechanics and thermodynamics (Lister and Kerr, 1991). Purely thermal models commonly assume an instantaneously emplaced dike of a given width, with initially uniform magma and host rock temperatures. Thermal evolution of dikes can be modeled assuming two concomitant processes: diffusion of heat across the dike, and advection of heat due to magma flow. Early models (e.g.,Wilson and Head, 1981), based on solutions of the thermal diffusion equation like those of Carslaw and Jaeger (1959), neglected the advective heat supply, which overestimates solidification and blocking of dikes. However, advection cannot be ignored, and a balance between advective and conductive heat fluxes reveals that the cooled region at the dike margins (thermal boundary layer) cannot exceed a given thickness (Delaney and Pollard, 1982; Bruce and Huppert, 1990; Lister and Kerr, 1991). Also, the portion of the dike over which this conduction-advection balance is established, which is initially close to the magma source, increases with time (Lister and Kerr, 1991). Important geological implications can be drawn from the analysis of the evolution of temperatures within the dike and its host rock. Those implications include critical width of dikes to prevent freezing, generation of chilled margins, remelting of chilled margins or dike walls, compositional and textural zonation of dikes (e.g.,Bruce and Huppert, 1989, 1990; Delaney and Pollard, 1982; Huppert and Sparks, 1989; Lister and Kerr, 1991), and granitoid magma transport or batholith-filling rates (e.g.,Clemens and Mawer, 1992; Petford etal., 1993, 2000), among others.

The temperature gradient generated across the thermal boundary layer not only leads to magma freezing and formation of chilled margins, but it can also have profound chemical consequences causing differentiation of silicic magmas. A process of geochemical fractionation of an original high-silica andesitic magma to generate a Qz-dioritic mush and a differentiated granitic melt, has been described and experimentally tested by Rodríguez and Castro (2017) through magma crystallization in a dynamic thermal gradient. Therefore, this work presents an application of a simple, first-order approximation to the problem of thermal evolution of dikes suffering differentiation. The results include viscosity and flow velocity profiles and allow us discussing the genesis of a range of magmatic structures commonly observed in ascent conduits and plutons, like autoliths, enclave corridors and swarms, double enclaves, schlieren, magmatic shear zones, back-veining structures, boudin-like structures, and zoned phenocrysts.

2. Semi-quantitative analysis of flow in ascent conduits subjected to geochemical splitting

2.1. Methodology

The procedure followed in this work considers a dike of half width ω (see Table 1 for a list of the main parameters and variables used in this work). The dike was emplaced instantaneously from a source region at depth, although magma continues to flow through it. The original composition of the magma is of a high-silica andesite (see below). Immediately after emplacement, the dike experiences rapid geochemical splitting and becomes compositionally divided in two zones with an abrupt change in composition (splitting): a Qz-dioritic mush on the margins and a differentiated granitic (sensu *lato*) melt in the interior. The model is based on the experimental results of Rodríguez and Castro (2017) simulating fractionation of a high-silica andesitic magma at the vertical walls of ascent conduits, where thermal gradients are normal to gravity. Those experiments evidenced that the fractionation process is more effective in the experiments with horizontal thermal gradients normal to gravity than in those performed to simulate gravity settling and compaction (Rodríguez and Castro, 2017). Therefore, in correspondence with the above-cited experiments, forces such as gravity or external deformation are not considered. As a result, compaction and gravity settling (e.g.,Bachmann and Bergantz, 2004) do not contribute in this particular case to magma fractionation. In the experiments of Rodríguez and Castro (2017), differentiation occurs through rapid lateral migration of a water-saturated silicate fluid (i.e.,a process similar to the gas-driven filter pressing of Pistone etal., 2015). The efficiency of the differentiation process has been evaluated, and it occurs in only a few hours inside the experimental capsules (Rodríguez and Castro, 2017). In natural silicic systems, and under the filter pressing mechanism, differentiation can occur within times

Table 1
List of parameters and variables used in this work, with indication of selected values (where appropriate) and their references.

Symbol	Meaning	Units	Value (ref.)
ω	Half width of the dike	m	–
ω_c	Critical half width	m	–
S_m, S_∞	Stefan numbers	(*)	–
L	Magma latent heat of solidification	$J.kg^{-1}$	3.35×10^5 (1)
c_p	Specific heat	$J.kg^{-1}.°C^{-1}$	1200 (1)
κ	Thermal diffusivity	$m^2.s^{-1}$	6.4×10^{-7} (2)
T_L	Initial magmatic temperature	°C	1100 (3)
T_i	Temperature at which the magma is effectively immobile	°C	875 (3)
T_H	Initial far-field temperature (host rock)	°C	400 (3)
η	Melt viscosity of the initial high-silica andesite magma	Pa.s	10^2 (3)
η_m	Melt viscosity (Qz-diorite and granite)	Pa.s	–
η_s	Magma viscosity (Qz-diorite and granite)	Pa.s	–
A	Distance from magma source to the point of observation	m	20,000 (3)
s	Distance travelled by the magma	m	–
g	Acceleration due to gravity	$m.s^{-2}$	9.8
Δ_ρ	Difference in density between the host crust and the initial high-silica andesite magma	$kg.m^{-3}$	340 (3)
y_{bl}	Thickness of the thermal boundary layer	m	–
P_e	Péclet number	(*)	–
f	Crystallinity	(*)	–
T'	Dimensionless temperature, $(T\text{-}T_S)/(T_L\text{-}T_S)$	(*)	–
T_l'	Dimensionless temperature at which one half of the magma has crystallized	(*)	0.5 (3)
σ_1	Standard deviation of T' about the most probable value of crystallinity	(*)	1 (4)
b	Scaling parameter for determining f	(*)	$30^{(1/2)}$ (4)
f_m	Concentration level of crystals for dense packing	(*)	0.7 (5)
B, n	Parameters of the empirical equation to estimate the viscosity of dense suspensions (5)	(*)	2.5, 2 (5)
V	Flow velocity inside the dike	$m.s^{-1}$	–
y	Distance from the dike wall to its center	m	–

(*) Dimensionless. Reference list: (1)Robertson (1988); (2)Eppelbaum etal. (2014); (3)this work; (4)Marsh (1981); (5)Dingwell etal. (1993).

several orders of magnitude shorter than the longevity of crystal mushes (Pistone etal., 2015). This very quick and highly efficient fractionation process was named by Rodríguez and Castro (2017) geochemical splitting— the term that will be used throughout this work—, in reference to the fact that fractionation splits the initial magma into two distinct subsystems with no gradational transitions between them: a crystal-rich cumulate or mush, and a fractionated liquid. According to experiments, this kind of differentiation operates in water-bearing magmas crystallizing in a thermal boundary layer. Note that this fractionation model differs from those based on crystal settling and compaction (e.g.,Dufek and Bachmann, 2010) in that crystals can remain relatively immobile during geochemical differentiation, and fractionation takes place primarily by expulsion of a water-rich fluid from the colder region (crystal mush) to the hotter, crystal-free, inner region of the dike. Although geochemical differentiation takes place in the cited experiments under static conditions of magma flow, the process is believed to be even more effective in a dike with magma continuously flowing through it (Rodríguez and Castro, 2017). The mechanical model outlined in this work considers a stage of dynamic equilibrium, with a fixed thermal boundary layer resulting from balance of heat advection and diffusion. It explores the rheological characteristics and the mechanical response of continued, steady state magma flow along an already differentiated dike. The model considers a horizontal, 1D transect, normal to the dike walls and at a given pressure (500 MPa, to fit the experiments of Rodríguez and Castro, 2017). No transient stages of cooling from the walls are here envisaged, although the effects of repeated intrusions and heating of country rocks are qualitatively explored.

In summary, the model starts from an emplaced and chemically differentiated dike, investigating the rheology and the kinematic effects of flow on the evolution of structures affecting chilled margins and generating mafic enclaves and enclave swarms. The first step followed here is to determine the critical width of the dike to prevent complete solidification. Then, the temperature profile close to the dike boundaries is established with approximate calculation of the thickness of the thermal boundary layer. Afterwards, the experimental results of Rodríguez and Castro (2017) are applied, including geochemical splitting across the temperature gradient. Finally crystallinity, viscosity, velocity and shear stress are computed along the 1D profile. The results allow us to discuss the generation of a number of magmatic structures associated with the origin of mafic enclaves and enclave swarms at magma ascent conduits.

Balance of advective and diffusive heat transfer has been semi-quantitatively modeled for a single transverse section of the dike at 500 MPa of lithostatic pressure, and located 20 km above the putative source region. The obtained temperature profile has been used, together with the geochemical variation expected at the studied transect according to the experiments by Rodríguez and Castro (2017), to determine crystallinity, viscosity and flow velocity profiles.

Distinct values of ω have been checked based on a minimum, critical value (ω_c) given by Petford etal. (1993):

$$\omega_c = 1.5\left(\frac{S_m}{S_\infty^2}\right)^{3/4}\left(\frac{\eta\kappa A}{g\Delta\rho}\right)^{1/4} \quad (1)$$

where S_m and S_∞ are Stefan numbers depending on the magma latent heat of solidification (3.35×10^5 J kg^{-1}) and specific heat (1200 J kg^{-1} °C^{-1}), the initial magmatic temperature (T_L = 1100 °C, Table 2), the temperature at which the magma is effectively immobile (860–875 °C, see below), and the far-field temperature of the host rock (T_H= 400 °C). On its turn, η is the initial melt viscosity (10^2 Pa s, see below), κ is the thermal diffusivity (6.4×10^{-7} m^2 s^{-1}), A is the distance from magma source to the point of observation (20 km), g is the acceleration due to gravity and Δp is the difference in density between the host crust (2700 kg m^{-3}) and the magma (2360 kg m^{-3} for the initial melt, see below). The assumption of instantaneous dike emplacement supports the use of the initial melt viscosity instead a bulk magma viscosity. Latent heat of solidification and specific heat (Robertson, 1988), and thermal diffusivity (Eppelbaum etal., 2014), are representative values for dioritic to Qz-dioritic magmas. The host density is an average value for a metasedimentary crust (Daly etal., 1966). Accordingly, the critical half width for the considered values is of around 0.3 m. Thick dikes should retain original dioritic magma flowing at their central parts, although the chemical splitting process still operates at their margins. Estimation of the Reynolds number indicates laminar flow within the dike for thicknesses well above the critical half width (ω_c). Initial values of melt viscosity, density, and maximum velocity (see below) suggests that laminar flow will predominate for $\omega \le 34$ m.

Table 2
Whole-rock chemical composition and liquidus and solidus temperatures of the starting material (AGV2) and derived products (Qz-diorite mush and differentiated granitic melt) for run CRH5 of Rodríguez and Castro (2017).

Rock type	AGV2	Qz-diorite	Differentiated granite
SiO_2	60.57	58.09	61.62
TiO_2	1.08	1.20	1.18
Al_2O_3	17.27	17.78	18.03
FeO_t	6.21	5.13	4.73
MgO	1.84	3.03	1.55
MnO	0.01	0.11	0.12
CaO	5.31	7.67	4.71
Na_2O	4.28	3.71	4.04
K_2O	2.94	2.43	3.35
P_2O_5	0.49	0.86	0.67
Total	100.00	100.00	100.00
Initial H_2O content (wt%)	4.00	4.00	4.00
Sat. H_2O content (wt%) (*)	8.50	9.50	9.50
T_L (*)	1100	1132	1070
T_S (*)	680	692	664

Chemical composition in wt% of oxides of major elements. Initial H_2O content: 4 wt%. Liquidus and solidus temperatures in °C. (*) Values determined with MELTS at 500 MPa (Asimow and Ghiorso, 1998; Ghiorso and Sack, 1995; Gualda etal., 2012). T_L: Liquidus temperature, T_S: Solidus temperature.

The initial temperature profile across the half width has been estimated with a first-order approximation determining first the thickness of the thermal boundary layer (y_{bl}) with the equation (Lister and Kerr, 1991):

$$y_{bl} \sim \left(\frac{\omega^2 s}{P_e}\right)^{1/3} \quad (2)$$

The Péclet number (P_e) is directly proportional to the half width of the dike and to the average fluid velocity along the dike, and inversely proportional to the thermal diffusivity. Average fluid velocity can be approximated from $\Delta\rho$, ω and (Petford etal., 1993). Accordingly, P_e can be given as:

$$P_e = \frac{g\Delta\rho\omega^3}{12\eta\kappa}. \quad (3)$$

Distance s travelled by the magma has been here equated to A. The thickness of the thermal boundary layer steeply increases with ω for values close to the critical half width, while the y_{bl}/ω ratio decreases for large dike thicknesses (Fig. 1). Given this variation, spatial coordinates have been made nondimensional by the thickness of the thermal boundary layer (y_{bl}). In a manner similar to Delaney and Pollard (1982), the temperature profile across the thermal boundary layer has been approximated as a linear function from the host-dike contact, where $T = (T_L\text{-}T_H)/2$, to the isothermal inner part of the dike, where $T = T_L$.

The benchmark run CRH5 of Rodríguez and Castro (2017) was produced using a stationary thermal gradient (from 1200 °C to 862 °C

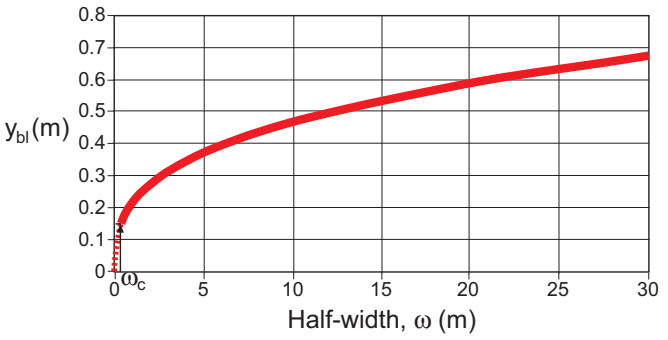

Fig. 1. Graph showing the variation of the thickness of the thermal boundary layer (y_{bl}) against the half-width of the dike (ω). See the main Text and Tables 1 and 2 for the values of the main controlling parameters. The dashed segment correspond to half-widths below the critical value (ω_c) to prevent complete solidfication of the dike.

across 9 mm), applied at 500 MPa during 315 h to the AGV2 standard high-silica (>60% SiO_2) andesite (Flanagan, 1967), with 4 wt% added water. The results of that run (crystallinity and compositional profiles as a function of temperature) are used here to analyze kinematic and structural evolution in ascent conduits. In particular, the temperature at which an abrupt compositional change was observed, indicating geochemical splitting, in run CRH5 is of 970 °C (Fig. 2a). Liquidus and solidus temperatures for AGV2, Qz-dioritic mush, and differentiated granite, as well as the initial melt density for AGV2, have been determined with MELTS code (Asimow and Ghiorso, 1998; Ghiorso and Sack, 1995; Gualda etal., 2012). Those data and the average chemical compositions of starting material and splitting products determined by Rodríguez and Castro (2017) and used in this work are shown in Table 2.

Calculation of the viscosities of the distinct crystallizing systems (AGV2, Qz-dioritic mush and differentiated granite) requires the previous determination of the viscosity of the silicate melt, which has been obtained following the approximation of Giordano etal. (2008), an optimized model accounting for both near-Arrhenian and non-Arrheniantemperature-dependent behaviors of a broad compositional range of silicate melts. Melt viscosities have been calculated for the entire range of temperatures between liquidus and solidus of each system, in steps of 1 °C. The initial (liquidus) water concentration in the melts is 4 wt%, in accordance with the experiment CRH5, and it has been recalculated as a consequence of the progressive crystallization of the investigated magmas, up to the saturation limit determined with MELTS(Table 2).

According to the empirical approach presented by Marsh (1981), the variation of crystallinity with decreasing temperature has been determined as follows:

$$f = \frac{1}{2}\left\{1 - \mathrm{erf}\left[\frac{b_1}{\sigma_1}(T' - T_l')\right]\right\} \quad (4)$$

with the dimensionless temperature (T) defined as:

$$T' = \frac{T - T_S}{T_L - T_S}, \quad (5)$$

where T_L and T_S are the liquidus and solidus temperatures, respectively. T_l' is the dimensionless temperature at which one half of the magma has crystallized. Here, T_l' is fixed at 0.5 (i.e. the temperature that exactly corresponds to the mid point between the liquidus and solidus temperatures). MELTS predicts comparable T_l' values for the studied compositions, within an error of ±10%. On its turn, σ_1 is related to the standard deviation of T about the most probable value of crystallinity and b_1 is a scaling parameter. According to the discussion by Marsh (1981), concerning the significance of these parameters, the following values have been chosen, $\sigma_1 = 1$ and $b_1 = (30)^{1/2}$. Again, all the intermediate temperatures between T_L and T_S, with intervals of 1 °C, have been considered. The theoretical temperature evolution of crystallinity for the three studied magmatic systems satisfactorily matches the experimental results (Fig. 2b).

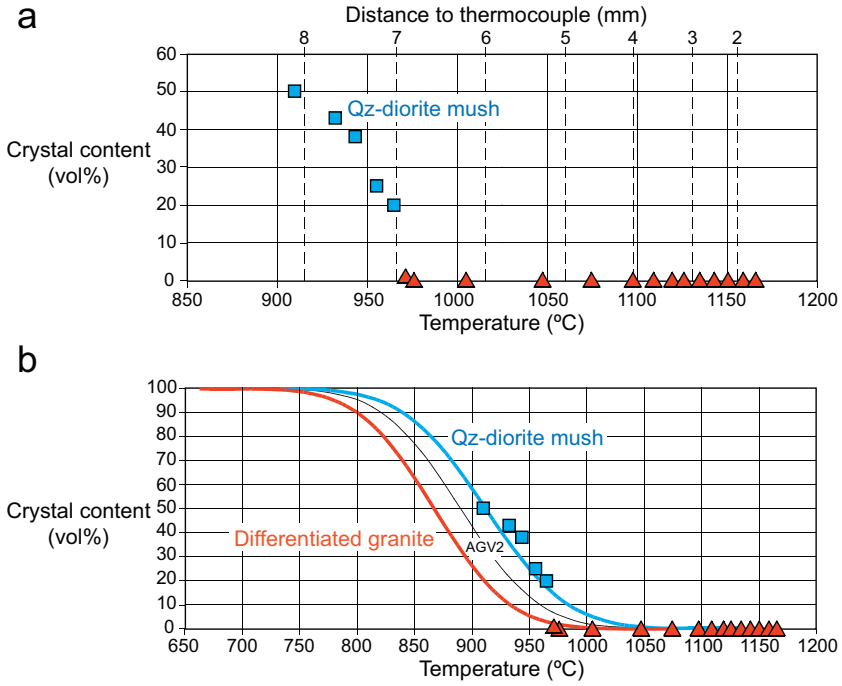

Fig. 2. (a)Crystal contents for the Qz-dioritic mush and differentiated granitic domains as a function of temperature. Data from experiment CRH5 of Rodríguez and Castro (2017). (b)Curves depicting the variation of crystal fraction with temperature for the starting material (AGV2) and its resulting products (Qz-dioritic mush and differentiated granite) of experiment CRH5, determined following the procedure explained in the main text. Actual values measured in experiment CRH5 are plotted for comparison.

The viscosity of the magma is directly dependent on melt viscosity, but the presence of crystals has a profound influence on magma rheology. For crystals contents in the range 0 and 10 vol% ($f < 0.1$), the Einstein's (1911) equation has been applied:

$$\eta_s = \eta_m(1 + 2.5f), \tag{6}$$

where η_m is the melt viscosity, as determined with the methodology of Giordano etal. (2008), and η_s is the magma viscosity. For crystallinity between 10 and 30 vol% ($0.1 < f < 0.3$) the Einstein-Roscoe equation (Einstein, 1911; Roscoe, 1952) has been used:

$$\eta_s = \eta_m\left(1 - \frac{f}{f_m}\right)^{-2.5}, \tag{7}$$

where f_m is the concentration level of crystals for dense packing, for which the shear viscosity of the system increases to infinity. Crystallinity for dense packing is dependent on several parameters, and varies between 0.52 and 0.74 for spheres (e.g. Dingwell etal., 1993). Here a value of 0.7 has been chosen for f_m. For denser suspensions ($0.3 < f < f_m$), Dingwell etal. (1993) proposed the following empirical equation:

$$\eta_s = \eta_m\left[1 + B\frac{\frac{f}{f_m}}{n\left(1 - \frac{f}{f_m}\right)}\right]^n, \tag{8}$$

with $B \approx 2.5$ for smooth-shaped particles, and $n \approx 2$ for strain rates corresponding to Newtonian behavior (Dingwell etal., 1993). The resulting viscosities for the three analyzed systems (AGV2, Qz-dioritic mush and differentiated granite, Fig. 3) are very similar for $T > 950$ °C, with a negative linear relationship between log(viscosity) and temperature. Approximate viscosity values vary from $10^{1.7}$ to $10^{3.5}$ Pa s, with slightly lower viscosities for the Qz-dioritic composition. In contrast, viscosities strongly differ at $T < 950$ °C, as a consequence of the distinct solidus temperatures and rates of crystal fraction variation with temperature. The viscosity of the Qz-dioritic system strongly increases approaching the solid-state value at ca. 875 °C, which takes place at 860 °C for AGV2 and 840 °C for the differentiated granite. The temperature of viscosity inversion for Qz-diorite and granite is of around 964 °C, i.e.,near the splitting temperature determined in experiment CRH5. Nondimensional viscosities are computed normalizing by the melt viscosity of the initial AGV2 magma.

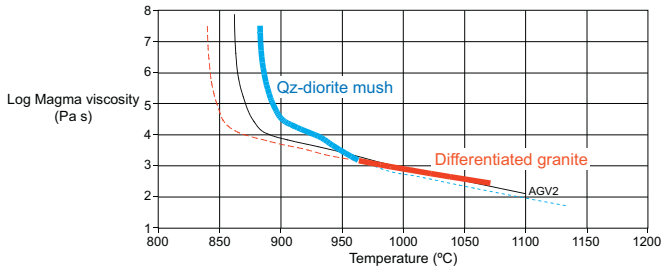

Fig. 3. Variation of magma viscosity with temperature for the high-silica andesite AGV2 and the two magmas resulting from the geochemical splitting experiment CRH5 of Rodríguez and Castro (2017): Qz-dioritic mush and differentiated granite. See main text for the calculation methodology. The profile is constructed taking into account the thermal gradient acquired during the initial stage of balance between heat diffusion across the dike and heat advection along it. Thick continuous lines indicate the theoretical viscosity profile across a dike where thermal gradient at the dike wall triggered geochemical splitting. Temperatures below 900 °C strongly increase the crystal fraction of Qz-dioritic mush, producing a pronounced viscosity gradient and, finally, hampering determination of magma viscosity.

The flow velocity has been calculated assuming Poiseuille flow inside the dike (e.g.,Malvern, 1969):

$$V = -\frac{1}{2}\Delta\rho g\left[\omega^2 - (y-\omega)^2\right]\frac{1}{\eta}, \tag{9}$$

where y is the distance from the dike wall to its center. Magma velocities have been normalized by the maximum flow velocity, corresponding to that of the initial AGV2 melt at the central part of the dike. Finally, the lateral variation of the shear stress (τ) resulting from the velocity gradient across the dike has been estimated assuming laminar flow (see above) as (e.g.,Malvern, 1969):

$$\tau = \eta_s\frac{\partial V}{\partial y}. \tag{10}$$

The resulting values of shear stress have been normalized by the experimentally determined maximum possible strength of partially molten granite for crystallinities of around 0.75 ($\approx$ 1 MPa, e.g. Rutter and Neumann, 1995), i.e.,just above the maximum crystal content value of the rheological threshold known as the solid-to-liquid transition or rheological critical melt percentage (Rosenberg and Handy, 2005; see below).

2.2. Results

Using this first-order approximation methodology it has been possible to construct profiles of the main relevant variables (nondimensional temperature, crystal fraction, viscosity, flow velocity, and shear stress) for a dike subjected to geochemical splitting (Fig. 4). The thickness of the thermal boundary layer has been normalized to the unity such that the resulting profiles are valid for any value of dike half width above ω_c. Crystal fraction remains very low ($f < 0.1$, i.e. <10 vol%) in the differentiated granitic melt. On the other hand, crystallinity approaches 0.2at the Qz-dioritic mush close to the splitting surface, while it attains 1.0 (mafic chilled margin) near the external contact of the dike (Fig. 4b). Therefore, both the solid-to-liquid transition (SLT) and the melt-connectivity transition (MCT) of Rosenberg and Handy (2005) are reached at the Qz-dioritic mush. The SLT describes the transition from a liquid- to a solid-supported rheology and is analogous to the rheological critical melt percentage of Arzi (1978). However, the greater strength variation of the magma system is related to the MCT (Rosenberg and Handy, 2005), corresponding to a crystal fraction of around 0.93. Magma viscosities increase across the thermal boundary layer, in parallel with the crystal fraction (Fig. 4c). No particular viscosity jump has been observed at the boundary between the granitic melt and the Qz-dioritic mush, as the effects of higher crystal fraction and lower melt viscosity relative to granitic melt cancel each other in the Qz-diorite. The SLT is marked by a strong viscosity gradient in the Qz-dioritic mush, while the effects of the MCT on the magma viscosity cannot be explored here, as the involved crystal fraction is larger than f_m. The typical parabolic flow velocity distribution of plane Poiseuille flow, evident in the central part of the dike, is truncated within the thermal boundary layer (Fig. 4d), and around 20–25% of the entire dike thickness (for values at or close to ω_c), near its external wall, becomes virtually stagnant. This kinematically frozen zone affects the Qz-dioritic mush, albeit a drastic decrease in flow velocity also affects the differentiated granitic melt. No sharp variation in flow velocity has been observed at the contact between Qz-dioritic and granitic systems. Flow shear stress increases from the central part of the dike, where it vanishes due to the absence of flow velocity gradients, towards its external boundary (Fig. 4e). A sharp increase in shear stresses is observed at the differentiated granitic melt inside the thermal boundary layer. A second step towards higher shear stress is verified at the interface between Qz-dioritic mush and differentiated granitic melt. Those steps in the shear stress profile are due to both the effects of strong velocity

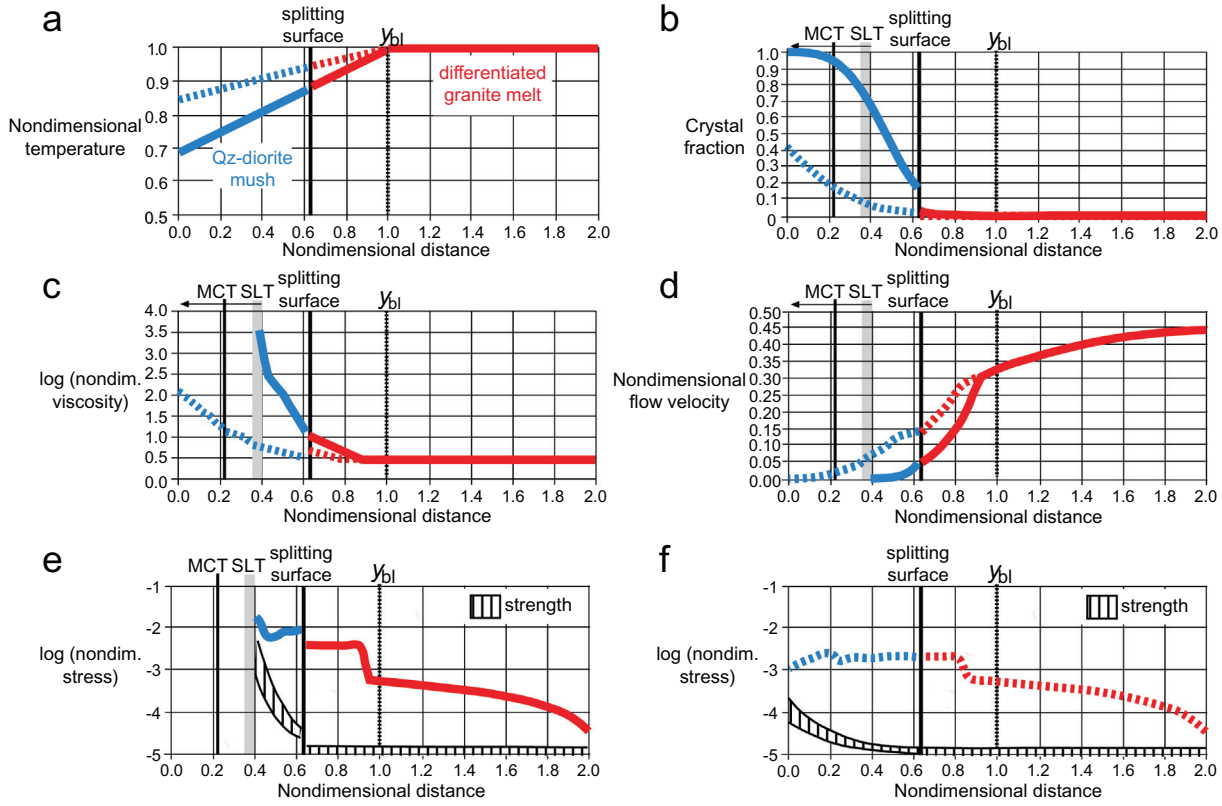

Fig. 4. Variation of critical thermal and mechanical parameters across the dike, based on the results of experiment CRH5 of Rodríguez and Castro (2017). See main text and Table2 for the values of the main controlling parameters. In all cases, the splitting surface marks the sudden change from the Qz-dioritic mush, at the dike margin, and the differentiated granitic melt at the inner part of dike. The nondimensional temperature and viscosity is normalized by the initial melt temperature and viscosity, respectively. The nondimensional distance is measured from the dike contact as a fraction of thickness of the thermal boundary layer (y_{bl}). The nondimensional flow velocity corresponds to magma velocity divided by the maximum initial flow velocity. The nondimensional shear stress due to flow is normalized by 1MPa (maximum strength at the solid-to-liquid transition, see main text). Continuous lines are the results for the balance between the loss of heat by diffusion and the supply of heat by advection. Discontinuous lines show the calculated gradients for an arbitrary stage of reheating and meltback (see main text for additional information). Rheological thresholds SLT (solid-to-liquid transition) and MCT (melt connectivity transition) are from Rosenberg and Handy (2005). Black arrows show their displacement towards the dike wall after reheating and meltback. The graphs show 1D gradients of temperature (a), crystal fraction (b), magma viscosity (c), flow velocity (d), and flow shear stress (e, f). Curves of granitic magma strength (e, f)are taken from Rosenberg and Handy (2005).

gradients and increases in magma viscosity. Finally, shear stresses strongly augment close to the SLT as a consequence of the sharp rise of magma viscosity.

Rising of host temperatures above half the temperature difference between the initial melt and far-field host temperatures is implicit in models predicting remelting of chilled margins and country rock (e.g., Bruce and Huppert, 1990). This is a consequence of the maintained flow within the dike such that heat flux from the magma exceeds the flux into the country rocks (Bruce and Huppert, 1989, 1990; Lister and Kerr, 1991). To approximately simulate this process, the far-field host rock temperature has been arbitrarily raised from 400 to 750 °C, and crystal fraction, magma viscosity and magma flow velocity profiles recalculated according to the new conditions (Fig. 4, dashed lines). The new host rock temperature was chosen to slightly exceed the curve of dehydration melting of typical crustal protoliths (e.g.,Castro etal., 2000; Patiño Douce and Harris, 1998; Thompson, 1982), therefore allowing partial melting of country rocks. As a consequence, crystal fraction of the Qz-dioritic mush suffers a dramatic reduction, with $f \approx 0.4$at the dike contact (Fig. 4b), resulting in remelting of the former chilled margin. The crystallinity jump at the splitting contact almost disappears. Both the SLT and the MCT vanish from the Qz-dioritic mush. Therefore, magma viscosity is reduced within the thermal boundary layer; with the Qz-dioritic mush less viscous than the granitic melt close to the splitting contact (Fig. 4c), thereby enhancing deformation localization within the Qz-dioritic mush near the interface with the differentiated granitic melt. On the other side, flow velocities tend to approach a parabolic profile (Fig. 4d). Shear stress remains relatively high within the thermal boundary layer, with only a minor drop near the external boundary of the dike (Fig. 4f). Taken together, these observations indicate that a sort of remobilization or rheomorphic process (Backlund, 1937; Reynolds, 1947) affecting the Qz-dioritic mush is possible, while the granitic melt is subjected to only minor changes.

Building of plutons and batholiths, as regions of magma accumulation, is an inherently episodic and incremental process taking place over hundred of thousands to millions of years (e.g.,Caricchi etal., 2016; Coleman etal., 2004; de Saint Blanquat etal., 2011; Glazner etal., 2004; Miller etal., 2009; Schaltegger etal., 2009; Zibra etal., 2014). Imaging of pluton feeding systems is mostly based on geophysical surveys (e.g.,Améglio and Vigneresse, 1999), owing to the rarity of exhumed subvertical feeding structures (e.g.,Pitcher, 1997). Detailed geophysical analysis of the three-dimensional shape of plutons commonly evidences a reduced number of narrow conduits acting as feeder zones (e.g., Améglio etal., 1997; Aranguren etal., 1997; Hecht and Vigneresse, 1999; Taylor, 2007). Independently from the exact nature of these feeder conduits, namely, self-propagating dikes or dike swarms, preexisting mechanical heterogeneities, active dilational structures in shear zones (see, e.g. Petford etal., 2000), the long-lasting, incremental growth of plutons probably requires reactivation of a common ascent conduit. In order to simulate the renewed use of a former dike, the original dike represented in Fig. 4 has been considered to become stagnant and cooled until the isotherm of 750 °C attains the center of the body, which implies a crystal fraction of 0.99 for the differentiated granitic system. A new magma pulse is then allowed to intrude across the central surface of the cooled and almost completely solidified dike,

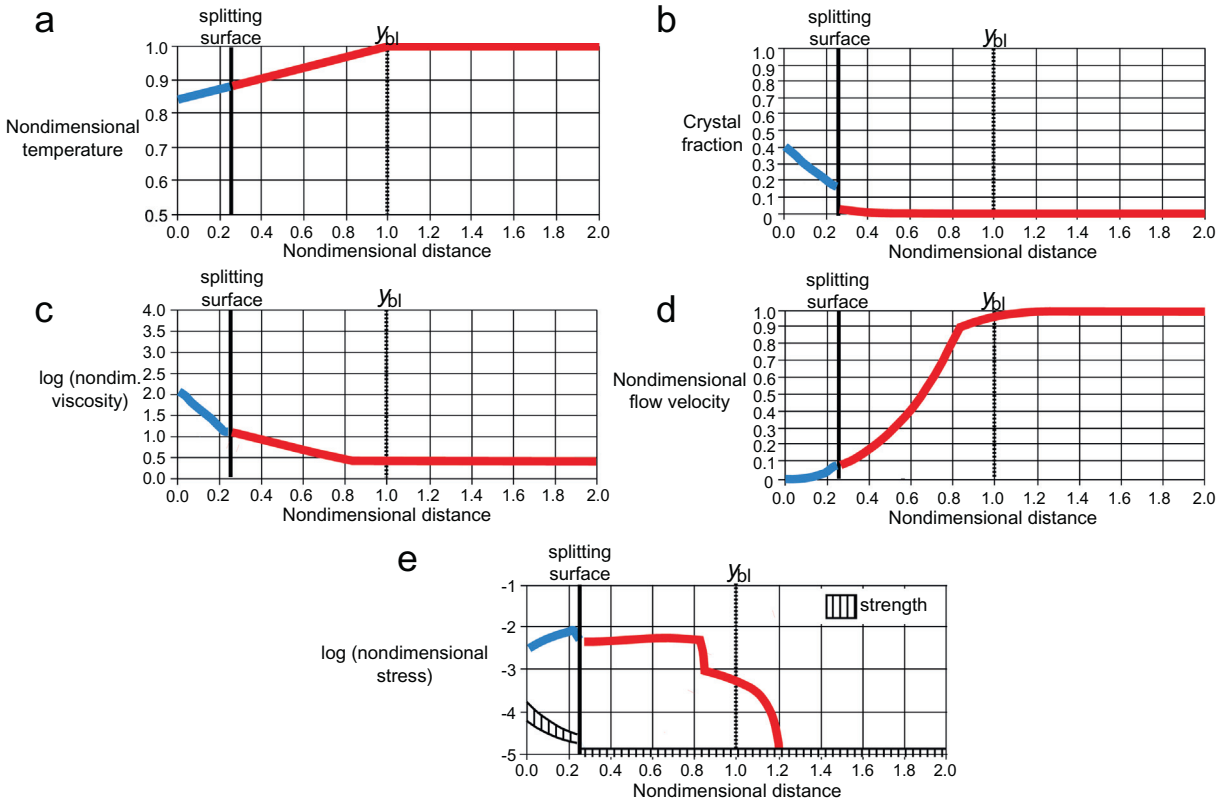

Fig. 5. Variation of critical thermal and mechanical parameters across the dike based on the results of experiment CRH5 of Rodríguez and Castro (2017), considering intrusion of a second Magma batch against the near completely crystallized old batch, whose central part remains at 750 °C. The graphs show gradients of nondimensional temperature (a), crystal fraction (b), and nondimensional Magma viscosity (c), flow velocity (d), and flow shear stress (e). See caption to Fig.4 for further information.

displacing it laterally. The thermal boundary layer developed in the new magma batch (Fig. 5a) originates geochemical splitting, a strong jump in crystal fraction across the splitting surface (Fig. 5b), marked viscosity and magma flow velocity gradients towards the contact with the old magma batch (Fig. 5c, d), and comparatively high shear stresses within the thermal boundary layer affecting both the Qz-dioritic mush and the granitic melt (Fig. 5e).

3. Discussion

3.1. Implications of the model

Flow velocity and magma viscosity profiles have been used to draw conceptual sketches showing the main textural (e.g.,crystal content and grain size) and structural expected implications resulting from the explored models. Once balance between heat advection and diffusion and geochemical splitting is accomplished within the dike, the Qz-dioritic mush exceeds the MCT (i.e.,$f > 0.93$) close to the dike wall (Fig. 6a), generating a chilled margin, characterized by fine grain size regions and a predominantly brittle behavior (Rosenberg and Handy, 2005). Differential stresses transmitted from the host rock, together with fluid pressure exerted from the interstitial melt (e.g.,Lister and Kerr, 1991), can be enough to promote transient brittle behavior of this near-solid carapace. Furthermore, because the intruding intermediate magma contains dissolved water, crystallization of the chilled margin is accompanied of excess fluid expulsion from the crystal-rich mush. Eventual propagation of faults or tensile structures will localize felsic residual melt and fluids in narrow veins that embrace angular fragments of Qz-dioritic mush (Fig. 6b); this is a first step in autolith generation. The size of the resulting fragments depends on the thickness of the brittle zone. For reasonable critical dike thicknesses, transverse dimensions of brittle fragments can range from a few centimeters to several decimeters (taking into account the relative sizes of the thermal boundary layer compared to reasonable dike half-width above ω_c represented in Fig. 1). Longitudinal lengths, parallel to the dike walls, are not restricted by thermal considerations and can be considerably larger. Existing data on average sizes of mafic enclaves and autoliths range from around 10^{-3} to 10^{0} m (e.g.,Barbarin, 2005; Barbey etal., 2008; Donaire etal., 2005; Hodge etal., 2012), which includes the effects of their formation and of later processes like magma flow and deformation (e.g.,Paterson etal., 2004; Williams and Tobisch, 1994). The enclave size estimations of this work are in accordance with the observed size range, albeit a rigorous numerical comparison with natural cases cannot be done due to those later processes modifying the enclave shapes and size ratios.

The SLT threshold is also verified within the Qz-dioritic mush (Fig. 6a). Deformation of the mush band located between the SLT and the MCT is more ductile and distributed than in the brittle area (Rosenberg and Handy, 2005), and becomes localized along a more or less interconnected network of melt-rich channels (Fig. 6b). Finally, a third rheological zone of the Qz-dioritic mush is located close to the interface with the differentiated granitic melt. In that area, with crystal fractions under the SLT, the solid framework breaks down enabling viscous behavior of the Qz-dioritic mush (see the gray-shaded area of the shear stress profile in Fig. 6a). The viscosity contrast between Qz-dioritic mush and granitic melt, albeit small, can trigger limited deformation of the splitting contact during flow, with cuspate-lobate forms, and even breakup of boudin-like or drop structures (Hodge etal., 2012; Laumonier etal., 2015) from the Qz-dioritic system into the granitic melt (Fig. 6b) that resemble symplutonic dikes and magma mingling structures. In fact, this is a kind of magma mingling in which the two involved magmas are cogenetic. The mingling model proposed by Bergantz (2000) may be illustrative to understand the complex process of mechanical interaction between the Qz-dioritic mush and the granitic

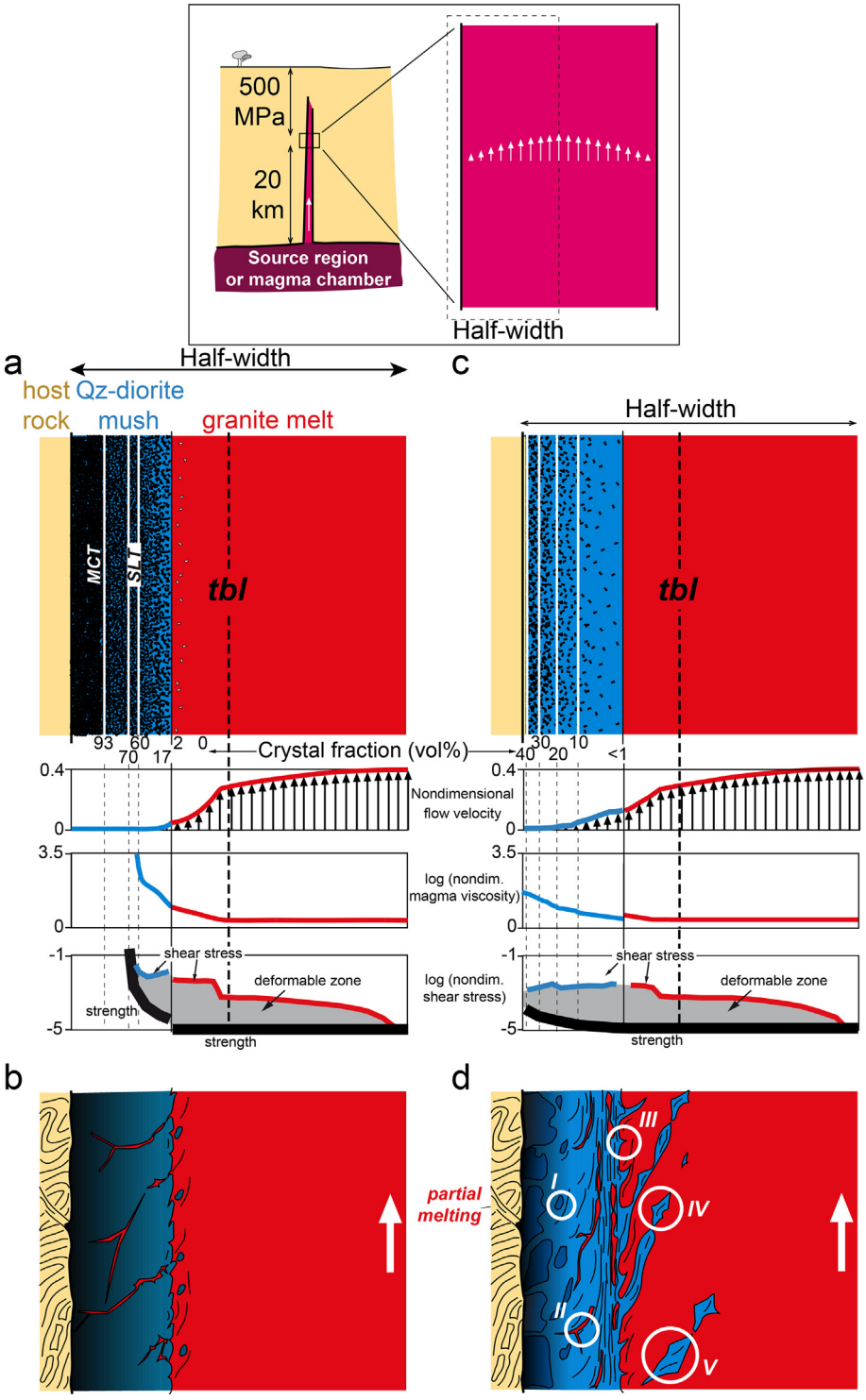

Fig. 6. Idealized sketches showing some mechanical and structural implications of the results. Inset shows the location within the crust of the modeled dike section, at a pressure of 500 MPa and 20 km above the magma source. The considered initial country rock temperature is 400 °C. The initial parabolic arrangement of flow velocities within the dike infilled with the AGV2 high-silica andesite, previously to the geochemical splitting is also depicted. The rectangle with a dashed border outlines the area enlarged in figures (a)to (d). After a temperature gradient is established across the thermal boundary layer (*tbl*) and geochemical splitting takes place, the results of Fig.4 allow constructing a snapshot image of the crystallinity variation in the Qz-dioritic mush and differentiated granitic melt (a). Taking into account magma viscosity and flow velocity, a sequence of structures can be predicted to develop in the dike margin (b). Reheating of the system by continued magma flow along the inner part of dike strongly reduces crystal fraction (c)and triggers melting back, and remobilization of previous structures (d). See main text for further explanation. The shaded areas in the shear stress profiles depict the viscous, deformable regions, i.e.,those where the calculated flow shear stresses exceed the magma strength. Points *I* to *V* in (d)show the hypothetical location on the sketch of some natural structures shown in Fig.8. Point *I*: Fig.8a, b; point *II*: Fig.8c; point *III*: Fig.8d; point *IV*: Fig.8f, g; point *V*: Fig.8 h, i.

melt at the border of the dike, despite the dynamic state of a dike subjected to a continuous flow of magma in its interior differs from the conditions considered by Bergantz (2000).

Reheating of dike walls leads to dramatic rheological changes, therefore modifying or even transposing the previous structures. Melting back of the Qz-dioritic mush reduces its crystallinity (Fig. 4b;

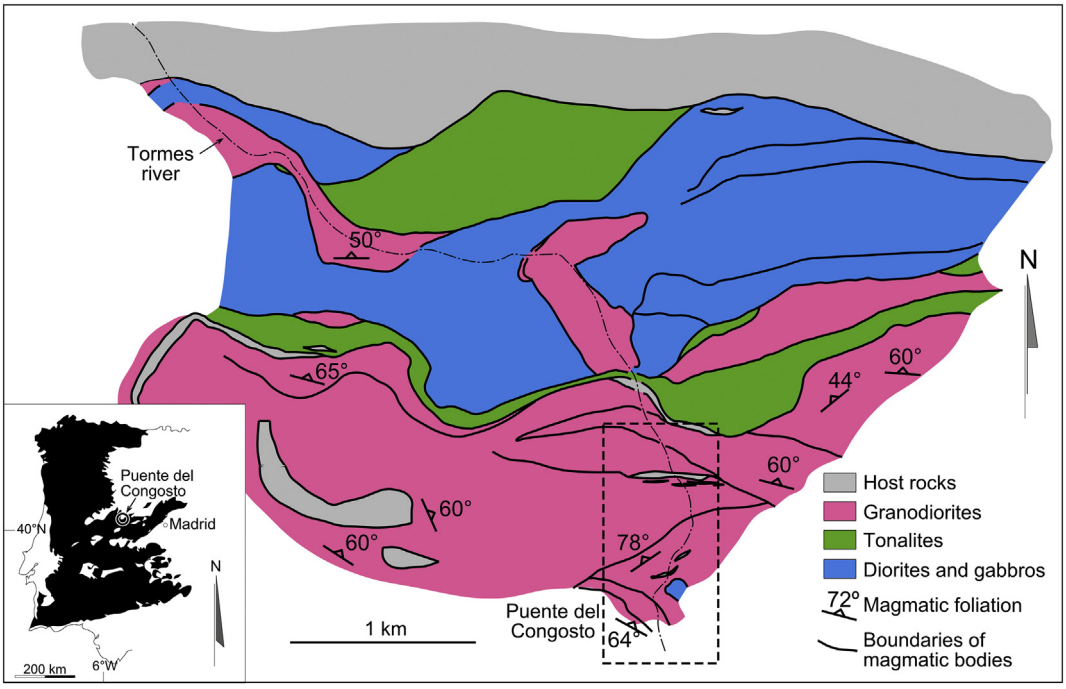

Fig. 7. Geological sketch of the Puente del Congosto area, at the northern boundary of the Spanish Central System batholith (modified from Fernández and Castro, 1999). Note the elongate, dike-shape form of the intruded granitic bodies, whose boundaries are mostly *E*-W oriented. The magmatic foliation and the contacts of the granitic bodies are highly dipping to subvertical. The dashed rectangle depicts the location of the photographs shown in Fig.8. The enclaves are concentrated at the boundaries of the successive magma batches. The inset shows the location of the Puente del Congosto area at the Variscan massif of Iberia.

Burgisser and Bergantz, 2011), forcing the SLT and MCT surfaces to migrate towards the dike walls, and even to eventually disappear (Fig. 6c). Magma viscosity strongly decreases in the Qz-dioritic mush, and a viscosity inversion is expected close to the splitting contact, where the viscosity of granitic melt can exceeds that of the Qz-dioritic system. The viscous deformable area enlarges to cover the entire thermal boundary layer up to the external boundary of the dike (cf. shear stress profile of Fig. 6c). This process allows entraining fragments of the former chilled margin.

3.2. Field examples

An excellent field case of lobate contacts indicating low viscosity of a Qz-dioritic system relative to a granitic melt can be found in the Central System batholith, Iberian massif (Figs.7 and 8d). Examples of the Spanish Central System batholith will be used in this discussion to illustrate many of the structures resulting from the proposed process of enclave and enclave swarm generation. In all cases, the examples are taken from a zone where multiple granitic magma batches intruded metasedimentary host rocks (Fig. 7). The granitic bodies in the selected zone (north of Puente del Congosto, Fig. 7) are elongate to tabular and dike-shaped, with highly dipping to subvertical contacts, while the enclaves and enclave swarms concentrate close to the external boundaries of each magmatic batch. These characteristics support the interpretation of most of the analyzed enclaves as formed by disintegration of dike margins. A channel of deformation localization appears at the granite-Qz-diorite contact (Fig. 6d), generating rapid remobilization and formation of highly foliated bands of Qz-dioritic mush (schlieren or" amoeboid" enclaves, Fig. 8f, g)that can become folded and kinematically mingled with the granitic melt. Relative viscosities predict cuspate-lobate interfaces with the granitic melt forming the lobes. Interestingly, the veinlets of granitic melt formed within the Qz-dioritic mush in the stage previous to remelting can develop boudin-like structures due to the competence inversion (Fig. 6d). Removal and partial resorption of large individual crystals during reheating can explain the formation of zoned plagioclase phenocrysts with repeated resorption and growth surfaces that characterize mafic microgranular enclaves (e.g.,Castro, 1990). Remelting of the chilled margin can be heterogeneous following previous flow structures or any heterogeneity. Thus, remelting may follow discrete veins (see above for their origin) isolating blocks that remain unchanged and that are the future mafic enclaves. Diffuse veins in which a sharp boundary cannot be identified are typical in many large enclaves that were dragged when they were in the process of disruption within the chilled margin of the feeder channel. Some enclaves of the Central System batholith may indeed represent a partially remelted zone of the rigid crust that formed at the external zone of the thermal boundary layer of a magma conduit (Fig. 8a, b). Blocks of the former chilled margins can be entrained within the rapidly flowing Qz-dioritic mush to yield autoliths, enclave swarms, and double enclaves (e.g. following the breakup mechanisms discussed by Hodge etal., 2012, or profiting previous brittle fractures). Double enclaves are also observed in the Iberian field cases mentioned above, where a Qz-dioritic enclave is embraced by fine-grained bands that represent soft mush portions of the same boundary layer (Fig. 8a, b). Leucocratic veins are indicative of brittle failure of the chilled margin (Fig. 8c). Also, large tabular enclaves with magmatic flow structures, representing disrupted mushes from the contacts with the intruding granitic host, are observed in the Central System batholith (Fig. 8 h, i). Those foliated blocks may represent a crystal-rich portion of the thermal boundary layer formed at the contact of magma pulses and finally broken apart and enclosed by the granitic magma. Similar processes of erosion of the chilled margin can result from transient or external processes like (Rodríguez and Castro, 2018): (1)increase in the ascent velocity of magma within the dike or (2)increase in the width of the channel (see below). However, the model discussed in this work predicts that remelting of the chilled margin to generate monogenic enclave swarms also occurs by maintained flow within the ascent channel (e.g.,Bruce and Huppert, 1990). Therefore, it can be anticipated that fragmentation of the chilled margins of ascent conduits is an inevitable process and it must be a universal mechanism of enclave generation in granitic systems.

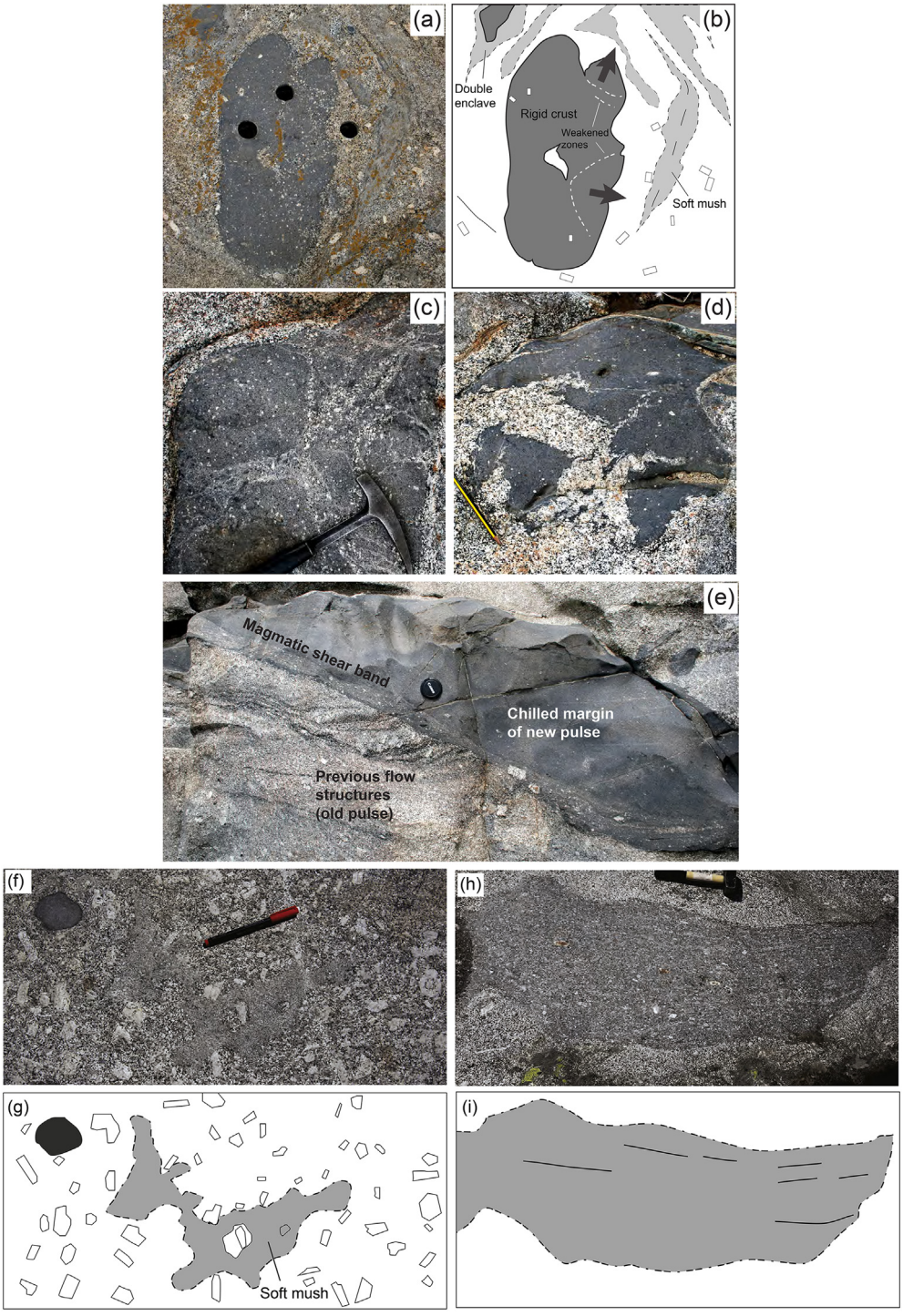

Fig. 8. Field relations of typical mafic microgranular enclaves in I-type granites of the Variscan massif of Iberia (Central System batholith). (a)Fine-grained enclave of Qz-dioritic composition containing phenocrysts of plagioclase, which are concentrated along bands or weakened zones (b), leading to disaggregation of the enclave in fragments by separation of the most crystalline parts, as indicated by black arrows in (b). Boreholes in (a)are 4 cm diameter. (c)Partially disaggregated fine-grained enclaves showing a network of leucocratic bands formed by remelting as in the former case. In this, fine-grained leucocratic veins are visible at the central left part of the outcrop. (d)Irregular fine-grained Qz-dioritic enclaves showing cuspate contacts with the host granite indicative of low viscosity compared with the host magma. Cuspate enclaves may represent Qz-dioritic liquids formed by remelting of a previously crystallized chilled margin (see Fig.6d). (e)Portion of the primitive contact of a new magma pulse with the corresponding chilled margin, intruding into a previously structured granitic mass. The thickness of the chilled margin is several decimeters, which is in agreement with that of the associated magma pulse (>30 m thick according to Fernández etal., 1997). (f)Irregular, "amoeboid" enclave of a fine-grained Qz-diorite enclosed in a porphyritic monzogranites. The boundaries are sharp at the scale of crystals, evidencing the magmatic state of two systems with similar viscosities. This represent a soft fragment of the mush region (g)from a primitive boundary layer formed at the sidewalls of an ascent conduit. (h)Large Qz-dioritic enclave showing magmatic flow structures (i).

Reheating also affects the host rock that can suffer partial melting (Bruce and Huppert, 1990). Leucosomes resulting from this process (Fig. 6d) are prone to mingle with magmas from the rapidly deforming dike wall (e.g.,Laumonier etal., 2015). More massive channeling of these anatectic melts inside the dike can explain the common observation of leucogranitic facies at the center of zoned plutons.

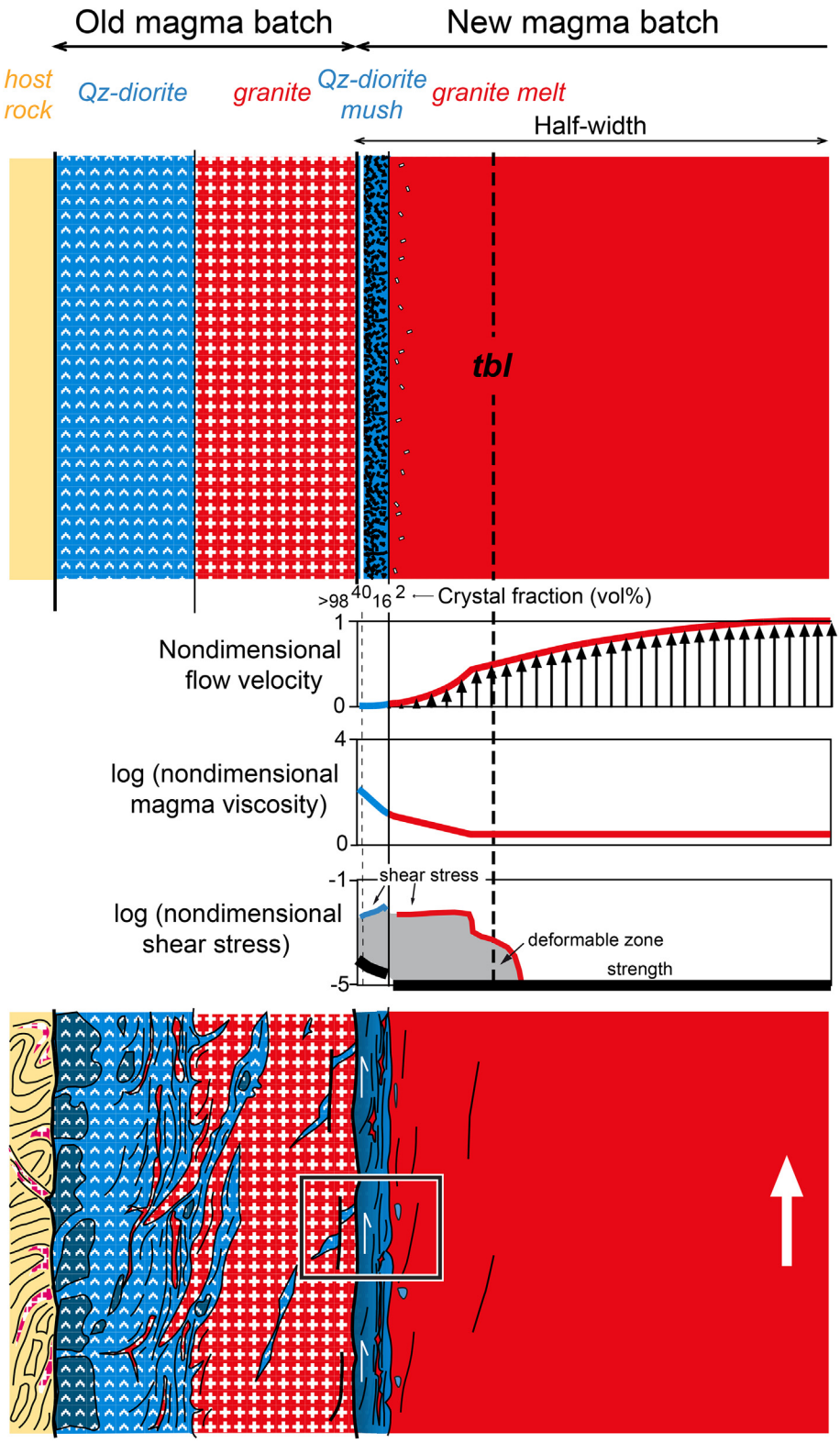

Fig. 9. Results of sequential emplacement of a new magma batch inside a nearly crystallized previous dike. See Fig.6 and main text for further explanation. The squared area in the lower sketch depicts the possible location of the geometry illustrated in the natural case of Fig.8e.

Reactivation of the dike with successive magma batches reproduces the same sequence of events giving place to new sets of magmatic structures (schlieren, enclaves and double enclaves, autoliths, boudin-like structures, magmatic shear zones) cross-cutting or remobilizing previous structures within the laterally growing ascent conduit (Fig. 9). Some good examples can be found in the Central System batholith, where new magma pulses, intruding into previous (not completely crystallized) magma batches, have been described elsewhere (Fernández etal., 1997). In some cases, a narrow magmatic shear band is formed at the contact (a deformable zone: see gray-shaded area at the shear stress profile of Fig. 9), while towards the interior of the new pulse (at the petrological splitting contact), viscosity contrasts

favor that fragments of the partially crystallized chilled margin are separated and incorporated to the granitic mass forming small rounded bodies (Fig. 8e, compare with Fig. 9). The new magma batch should also modify the thermal and rheological characteristics of its nearly crystallized magmatic host (e.g, see the deformed flow structure of the old pulse in Fig. 8e), although such a process has not been specifically addressed in this work.

3.3. Limitations of the model

Apart from the explanation of distinct types of magmatic structures in granitic plutons and batholiths, including the origin of some mafic microgranular enclaves, the model faces some difficulties to be used as a general methodology to interpret conditions of emplacement from field observations. The considered lithostathic pressure (500 MPa) and composition of the initial melt (high-silica andesite) are a consequence of the available experimental data that provide the necessary geochemical information for the model (Rodríguez and Castro, 2017). Also the distance above the magma source (20 km), and the initial country rock temperature (400 °C), are external variables whose exact value can significantly influence the final results. The assumptions of instantaneous dike emplacement and fast geochemical splitting as previous steps for the mechanical interactions described in this work constitute a first approach to a more complex process. Nevertheless, no analytical solutions are available to deal with the simultaneous interaction of flow, cooling and fractionation processes. Ascent conduits are complex, 3D structures, and a complete knowledge of the processes taking place along their entire length, from the source to the final emplacement level, is needed. Departures from steady-state conditions due to external stress sources, partial blocking of the conduit, increase or decrease of the magma velocity at the internal part of the dike, and geochemical changes in the original magma composition, among many other causes, should be also examined in more comprehensive models. Therefore, the results of this work must be taken as a first approximation to a more general problem. New experimental and theoretical work, as well as detailed field observations, is the prerequisite for obtaining more refined and robust models, able to rigorously explain the complex evolution of the ascent conduits in granitic systems.

4. Conclusions

This work shows the results of a first-order approximation to the problem of thermal and mechanical evolution of a silicic magma ascending through a dike that suffered geochemical splitting by crystal-liquid separation. According to this process, an original high-silica andesite magma is separated into a Qz-dioritic mush at the outer margin of a magma ascent conduit and a differentiated granitic melt at its center. Following the thermal balance between heat advection and diffusion, crystal fractions are low ($f < 0.1$ close to the chemical splitting surface) in the granitic melt, albeit high crystallinities are attained in the dioritic mush.

Once balance between heat advection and diffusion and geochemical splitting is accomplished within the dike, both the solid-to-liquid and melt-connectivity rheological transitions are reached in the Qz-dioritic mush, and a Qz-dioritic chilled margin ($f > 0.93$) appears at the external contacts of the conduit. Brittle failure of this chilled margin can result from the activity of differential stresses associated with the dike and host-rock dynamics, which is a first stage in the generation of mafic enclaves (autoliths). Remelting of the frozen zone due to the maintained flow within the dike not only reduces the crystallinity of the Qz-dioritic mush, but it also has drastic effects on the rheology of the ascending magma. As a consequence, the Qz-dioritic body behaves as a remobilized band able to further fragment the chilled margin and to entrain the resulting mafic enclaves forming schlieren, enclave swarms, boudin-like structures, rheomorphic bands, and double enclaves, among other magmatic structures. Sequential reactivation of the ascent conduit with successive magma batches can give place to a wide variety of transposing, cross-cutting or remobilizing structures at the final emplacement level. More general models are needed to fully explain the complex mechanical and geochemical evolution of the ascent conduits that feed the large granitic plutons and batholiths.

Acknowledgements

This research was funded by the Spanish Agency of Science and Technology (Project CGL2013-48408-C3-1-P) and the University of Huelva. Careful and constructive reviews by Benjamin Andrews, Jirí Žák, and an anonymous reviewer greatly improved the original manuscript, and are gratefully acknowledged.

References

Améglio, L., Vigneresse, J.L., 1999. Geophysical imaging of the shape of granitic intrusions at depth: a review. In: Castro, A., Fernández, C., Vigneresse, J.L. (Eds.), Understanding Granites: Integrating New and Classical Techniques. Geological Society, London, Special Publications. Vol. 168, pp. 39–54.

Améglio, L., Vigneresse, J.L., Bouchez, J.L., 1997. Granite pluton geometry and emplacement mode inferred from combined fabric and gravity data. In: Bouchez, J.L., Hutton, D.H.W., Stephens, W.E. (Eds.), Granite: From Segregation of Melt to Emplacement Fabrics. Kluwer Academic Publishers, Dordrecht, pp. 199–214.

Aranguren, A., Larrea, F.J., Carracedo, M., Cuevas, J., Tubía, J.M., 1997. The Los Pedroches batholith (southern Spain): polyphase interplay between shear zones in transtension and setting of ranites. In: Bouchez, J.L., Hutton, D.H.W., Stephens, W.E. (Eds.), Granite: From Segregation of Melt to Emplacement Fabrics. Kluwer Academic Publishers, Dordrecht, pp. 215–229.

Arzi, A., 1978. Critical phenomena in the rheology of partially melted rocks. Tectonophysics 44, 173–184.

Asimow, P.D., Ghiorso, M.S., 1998. Algorithmic modifications extending MELTS to calculate subsolidus phase relations. American Mineralogist 83, 1127–1132.

Bachmann, O., Bergantz, G.W., 2004. On the Origin of Crystal-poor rhyolites: Extracted from Batholithic Crystal Mushes. Journal of Petrology 45, 1565–1582.

Backlund, H., 1937. Die Umgrenzung der Svekofenniden. Bulletin of the Geological Institution of the University of Upsala 27, 219–269.

Barbarin, B., 2005. Mafic magmatic enclaves and mafic rocks associated with some granitoids of the Central Sierra Nevada batholith, California: nature, origin, and relations with the hosts. Lithos 80, 155–177.

Barbarin, B., Didier, J., 1991. Review of the Main Hypotheses Proposed for the Genesis and Evolution of Mafic Microgranular Enclaves. In: Didier, J., Barbarin, B. (Eds.), Enclaves and Granite Petrology, Developments in Petrology. Vol. 13. Elsevier, Amsterdam, pp. 367–373.

Barbarin, B., Didier, J., 1992. Genesis and evolution of mafic microgranular enclaves through various types of interaction between coexisting felsic and mafic magmas. Transactions of the Royal Society of Edinburgh: Earth Sciences 83, 145–153.

Barbey, P., Gasquet, D., Pin, C., Bourgeix, A., 2008. Igneous banding, Schlieren and mafic enclaves in calc-alkaline granites: the Budduso pluton, Sardinia. Lithos 104, 147–163.

Bergantz, G.W., 2000. On the dynamics of magma mixing by reintrusion: implications for pluton assembly processes. Journal of Structural Geology 22, 1297–1309.

Bruce, P.M., Huppert, H.E., 1989. Thermal control of basaltic fissure eruptions. Nature 342, 665–667.

Bruce, P.M., Huppert, H.E., 1990. Solidification and melting along dykes by the laminar flow of basaltic magma. In: Ryan, M.P. (Ed.), Magma Transport and Storage. John Wiley & Sons, pp. 87–101.

Burgisser, A., Bergantz, G.W., 2011. A rapid mechanism to remobilize and homogenize highly crystalline magma bodies. Nature 471, 212–215.

Caricchi, L., Simpson, G., Schaltegger, U., 2016. Estimates of volume and magma input in crustal magmatic systems from zircon geochronology: the effect of modeling assumptions and system variables. Frontiers in Earth Science 4, 48. https://doi.org/10.3389/feart.2016.00048.

Carslaw, H.S., Jaeger, J.C., 1959. Conduction of Heat in Solids. Vol. 520. Oxford University Press, Oxford pp.

Castro, A., 1990. Microgranular enclaves of the Quintana granodiorite (Los Pedroches batholith) Petrogenetic significance. Revista de la Sociedad Geológica de España 3, 7–21.

Castro, A., Corretgé, L.G., El-Biad, M., El-Hmidi, H., Fernández, C., Patiño Douce, A.E., 2000. Experimental constraints on Hercynian anatexis in the Iberian Massif, Spain. Journal of Petrology 41, 1471–1488.

Castro, A., Martino, R., Vujovich, G., Otamendi, J., Pinotti, L., D'Eramo, F., Tibaldi, A., Viñao, A., 2008. Top-down structures of mafic enclaves within the Valle Fértil magmatic complex (early Ordovician, San Juan, Argentina). Geologica Acta 6, 217–229.

Clemens, J.D., Mawer, C.K., 1992. Granitic magma transport by fracture propagation. Tectonophysics 204, 339–360.

Coleman, D.S., Gray, W., Glazner, A.F., 2004. Rethinking the emplacement and evolution of zoned plutons: geochronologic evidence for incremental assembly of the Tuolumne Intrusive Suite, California. Geology 32, 433–436.

Daly, R.A., Manger, G.E., Clark, S.P., 1966. Density of Rocks. In: Clark, S.P. (Ed.), Handbook of Physical Constants. Vol. 97, pp. 19–26 Geological Society of America, Memoir.

de Saint Blanquat, M., Horsman, E., Habert, G., Morgan, S., Vanderhaeghe, O., Law, R., Tikoff, B., 2011. Multiscale magmatic cyclicity, duration of pluton construction, and the paradoxical relationship between tectonism and plutonism in continental arcs. Tectonophysics 500, 20–33.
Delaney, P.T., Pollard, D.D., 1982. Solidification of basaltic magma during flow in a dike. American Journal of Science 282, 856–885.
Dingwell, D.B., Bagdassarov, N.S., Bussod, G.Y., Webb, S.L., 1993. Magma rheology. In: Luth, R.W. (Ed.), Short Handbook on Experiments at High Pressure and Applications to Earth's Mantle. Mineralogical Association of Canada. Vol. 21, pp. 131–196.
Donaire, T., Pascual, E., Pin, C., Duthou, J.L., 2005. Microgranular enclaves as evidence of rapid cooling in granitoid rocks: the case of the Los Pedroches granodiorite, Iberian Massif, Spain. Contributions to Mineralogy and Petrology 149, 247–265.
Dufek, J., Bachmann, O., 2010. Quantum magmatism: magmatic compositional gaps generated by melt-crystal dynamics. Geology 38, 687–690.
Einstein, A., 1911. Eine neue Bestimmung der Moleküldimensionen. Ann. Phys. 19, 289–306.
Eppelbaum, L., Kutasov, I., Pilchin, A., 2014. Applied Geothermics. Springer-Verlag, Berlin (732 pp).
Fernandez, A.N., Barbarin, B., 1991. Relative rheology of coexisting mafic and felsic magmas: Nature of resulting interaction processes. Shape and mineral fabricsof mafic microgranular enclaves. In: Didier, J., Barbarin, B. (Eds.), Enclaves and Granite Petrology, Developments in Petrology. Vol. 13. Elsevier, Amsterdam, pp. 263–275.
Fernández, C., Castro, A., 1999. Brittle behaviour of granite magma: the example of Puente del Congosto, Iberian Massif, Spain. In: Castro, A., Fernández, C., Vigneresse, J.L. (Eds.), Understanding Granites: Integrating New and Classical Techniques. Vol. 168, pp. 191–206 Geological Society, London, Special Publications.
Fernández, C., Castro, A., de la Rosa, J.D., Moreno-Ventas, I., 1997. Rheological aspects of magma transport inferred from rock structures. In: Bouchez, J.L., Hutton, D.H.W., Stephens, W.E. (Eds.), Granite: From Segregation of Melt to Emplacement Fabrics. Kluwer Academic Publishers, Dordrecht, pp. 75–91.
Fershtater, G.B., Borodina, N.S., 1977. Petrology of autoliths in granitic rocks. International Geology Review 19, 458–468.
Flanagan, F.J., 1967. U.S. Geological Survey silicate rock standards. Geochimica et Cosmochimica Acta 31, 289–308.
Frost, T.P., Mahood, G.A., 1987. Field, chemical, and physical constraints on mafic-felsic magma interaction in the Lamarck granodiorite, Sierra Nevada, California. Geological Society of America Bulletin 99, 272–291.
Ghiorso, M.S., Sack, R.O., 1995. Chemical Mass transfer in Magmatic Processes. IV. A revised and Internally Consistent Thermodynamic Model for the Interpolation and Extrapolation of Liquid-Solid Equilibria in Magmatic Systems at Elevated Temperatures and Pressures. Contributions to Mineralogy and Petrology 119, 197–212.
Giordano, D., Rusell, J.K., Dingwell, D.B., 2008. Viscosity of magmatic liquids: a model. Earth and Planetary Science Letters 271, 123–134.
Glazner, A.F., Bartley, J.M., Coleman, D.S., Gray, W., Taylor, Z.T., 2004. Are plutons assembled over millions of years by amalgamation from small magma chambers. GSA Today 14, 4–11.
Gualda, G.A.R., Ghiorso, M.S., Lemons, R.V., Carley, T.L., 2012. RhyoliteMELTS: a modified calibration of MELTS optimized for silica-rich, fluidbearing magmatic systems. Journal of Petrology 53, 875–890.
Hecht, L., Vigneresse, J.L., 1999. A multidisciplinary approach combining geochemical, gravity and structural data: implications for pluton emplacement and zonation. In: Castro, A., Fernández, C., Vigneresse, J.L. (Eds.), Understanding Granites: Integrating New and Classical Techniques. Vol. 168, pp. 95–110 Geological Society, London, Special Publications.
Hodge, K.F., Carazzo, G., Jellinek, A.M., 2012. Experimental constraints on the deformation and breakup of injected magma. Earth and Planetary Science Letters 325-326, 52–62.
Huppert, H.E., Sparks, R.S.J., 1989. Chilled margins in igneous rocks. Earth and Planetary Science Letters 92, 397–405.
Huppert, H.E., Sparks, R.S.J., Turner, J.S., 1984. Some effects of viscosity on the dynamics of replenished magma chambers. Journal of Geophysical Research 89B, 6857–6877.
Laumonier, M., Scaillet, B., Arbaret, L., Andújar, J., Champallier, R., 2015. Experimental mixing of hydrous magmas. Chemical Geology 418, 158–170.
Lister, J.R., Kerr, R.C., 1991. Fluid-mechanical models of crack propagation and their application to magma transport in dykes. Journal of Geophysical Research 96, 10049–10077.
Malvern, L.E., 1969. Introduction to the Mechanics of a Continuum Medium. Prentice-Hall. Englewood Cliffs, New York, p. 713.
Marsh, B.D., 1981. On the crystallinity, probability of occurrence, and rheology of lava and magma. Contributions to Mineralogy and Petrology 78, 85–98.
Miller, C.F., Furbish, D.J., Walker, B.A., Claiborne, L.L., Koteas, G.C., Bleick, H.A., Miller, J.S., 2009. Growth of plutons by incremental emplacement of sheets in crystal-rich host: evidence from Miocene intrusions of the Colorado River region, Nevada. USA. Tectonophysics 500, 65–77.
Paterson, S.R., 2009. Magmatic tubes, pipes, troughs, diapirs, and plumes: late-stage convective instabilities resulting in compositional diversity and permeable networks in crystal-rich magmas of the Tuolumne batholith, Sierra Nevada, California. Geosphere 5, 496–527.
Paterson, S.R., Pignotta, G.S., Vernon, R.H., 2004. The significance of microgranitoid enclave shapes and orientations. Journal of Structural Geology 26, 1465–1481.
Patiño Douce, A., Harris, N., 1998. Experimental constraints on Himalayan anatexis. Journal of Petrology 39, 689–710.
Petford, N., Kerr, R.C., Lister, J.R., 1993. Dike transport of granitoid magmas. Geology 21, 845–848.
Petford, N., Cruden, A.R., McCaffrey, J.W., Vigneresse, J.L., 2000. Granite magma formation, transport and emplacement in the Earth's crust. Nature 408, 669–673.
Pistone, M., Arzilli, F., Dobson, K.J., Cordonnier, B., Reusser, E., Ulmer, P., Marone, F., Whittington, A.G., Mancini, L., Fife, J.L., Blundy, J.D., 2015. Gas-driven filter pressing in magmas: Insights into in-situ melt segregation from crystal mushes. Geology 43, 699–702.
Pitcher, W.S., 1991. Synplutonic dykes and mafic enclaves. In: Didier, J., Barbarin, B. (Eds.), Enclaves and granite petrology, Developments in Petrology. Vol. 13. Elsevier, Amsterdam, pp. 383–391.
Pitcher, W.S., 1997. The Nature and Origin of Granite. second ed. Vol. 387. Chapman & Hall, London.
Reynolds, D.L., 1947. The granite controversy. Geological Magazine 84, 209–223.
Robertson, E.C., 1988. Thermal Properties of Rocks. United States Geological Survey. Open-File Report 88-441, 106.
Rodríguez, C., Castro, A., 2017. Silicic magma differentiation in ascent conduits. Experimental constraints. Lithos 272-273, 261–277.
Rodríguez, C., Castro, A., 2018. Origins of mafic microgranular enclaves and enclave swarms in granites: Field and geochemical relations. Geological Society of America Bulletin (in press).
Roscoe, R., 1952. The viscosity of suspensions of rigid spheres. British Journal of Applied Physics 3, 267–269.
Rosenberg, C.L., Handy, M.R., 2005. Experimental deformation of partially melted granite revisited: implications for the continental crust. Journal of Metamorphic Geology 23, 19–28.
Rutter, E., Neumann, D.H.K., 1995. Experimental deformation of partially molten Westerly granite under fluid-absent conditions, with implications for the extraction of granitic magmas. Journal of Geophysical Research 100, 15697–15715.
Schaltegger, U., Brack, P., Ovtcharova, M., Peytcheva, I., Schoene, B., Stracke, A., Marocchi, M., Bargossi, G.M., 2009. Zircon and titanite recording 1.5 million years of magma accretion, crystallization and initial cooling in a composite pluton (southern Adamello batholith, northern Italy). Earth and Planetary Science Letters 286, 208–218.
Sparks, R.S.J., Sigurdsson, H., Wilson, L., 1977. Magma mixing: a mechanism for triggering acid explosive eruptions. Nature 267, 315–318.
Taylor, G.K., 2007. Pluton shapes in the Cornubian Batholith: new perspectives from gravity modelling. Journal of the Geological Society, London 164, 525–528.
Thompson, A.B., 1982. Dehydration melting of pelitic rocks and the generation of H_2O-undersaturated granitic liquids. American Journal of Science 282, 1567–1595.
Vernon, R.H., 1983. Restite, xenoliths and microgranitoid enclaves in granites. Journal and Proceedings of the Royal Society of New South Wales 116, 77–103.
White, A.J.R., Chappell, B.W., Wyborn, D., 1999. Application of the restite model to the Deddick granodiorite and its enclaves. A reinterpretation of the observations and data of Maas etal. (1997). Journal of Petrology 40, 413–421.
Wiebe, R.A., Jellinek, M., Markley, M.J., Hawkins, D.P., Snyder, D., 2006. Steep Schlieren and associated enclaves in the Vinalhaven granite, Maine: possible indicators for granite rheology. Contributions to Mineralogy and Petrology 153, 121–138.
Williams, Q., Tobisch, O.T., 1994. Microgranitic enclave shapes and magmatic strain histories: constraints from drop deformation theory. Journal of Geophysical Research 99 (B12), 24359 (doi:19.1029/94JB01940).
Wilson, L., Head, J.W., 1981. Ascent and eruption of basaltic magma on the Earth and Moon. Journal of Geophysical Research 86, 2971–3001.
Zibra, I., Smithies, R.H., Wingate, M.T.D., Kirkland, C.L., 2014. Incremental pluton emplacement during inclined transpression. Tectonophysics 623, 100–122.